APPLICATIONS OF
MODELLING AND SIMULATION
http://arqiipubl.com/ams eISSN 2600-8084 VOL 6, 2022, 49-63

Development of Flight Dynamics Model for AH-25 Hybrid Unmanned Aerial Vehicle

Osichinaka C. Ubadike[1], Khalid K. Dandago[1*], Mahmud S. Zango[1], Ameer Mohammed[2], P. P. Okonkwo[1], T. D. Chollom[1], Bashir B. Muhammed[2], Christopher O. Adeboye[2]

[1]Aerospace Engineering Department, Air Force Institute of Technology, Kaduna, Nigeria
[2]Mechatronic Engineering Department, Air Force Institute of Technology, Kaduna, Nigeria

[*]Corresponding author: khaliddandago@gmail.com

Submitted 12 January 2022, Revised 01 March 2022, Accepted 22 March 2022, Available online 06 June 2022.

Abstract: A good mathematical model accurately represents the behavior of a system. Although aircraft has complex dynamics, it is feasible to develop a robust model that could be used to design and analyze some of its essential components such as flight control system and simulator. To solve security challenges in the hinterlands and maritime domains, a hybrid Unmanned Aerial Vehicle (UAV), nicknamed 'AH-25', was designed by the Air Force Institute of Technology, Nigeria. In this work, the development of flight dynamics models of the vehicle is presented. The AH-25 UAV has the capability of operating in both fixed-wing and Vertical Take-Off and Landing (VTOL) modes for effective operations on land and maritime spaces. Therefore, models that capture the dynamics of the two distinct modes were obtained. The fixed-wing nonlinear model which was developed from first principle using Newton-Euler method was decoupled, trimmed and linearized to set it in a good shape for critical aircraft systems designs. On the other hand, the multicopter model developed by Beihang flight control group was adapted for modelling the VTOL mode. Simulation results showed that the models' responses are a replica of the actual aircraft operations. Also, responses of the model to perturbations indicated that it is open-loop stable. Furthermore, the mean performance metrics of the fixed-wing model's open-loop time response to various inputs were evaluated. The model was found to have a rise time of 2 s, 1.33% steady state error and a settling time of 40 s.

Keywords: Flight dynamics; Mathematical model; Newton-Euler method; Unmanned aerial vehicle.

1. INTRODUCTION

Military operations with Unmanned Aerial Vehicles (UAVs) are evolving by the day. Surveillance, mission planning and combat are among a host of military activities that are executed with UAVs [1-2]. In its bid to address some of the operational challenges of the Nigerian military, the Air Force Institute of Technology (AFIT), Nigeria, has designed an UAV which is nicknamed 'AH-25'. The UAV is a product of the yearly Group Design Project (GDP) that is part of AFIT's M.Eng. curriculum for Aerospace Engineering.

The AH-25 Hybrid UAV was designed to: 1) Deliver critical lifesaving medical supplies to soldiers in an austere environment. 2) Perform search and rescue missions in a maritime environment. 3) Secure valuable assets of Nigeria's territorial and exclusive economic zones. Figure 1 shows a model of the aircraft. The AH-25 UAV is required to be a long endurance UAV with capability of 5 kg payload, and perform its operation safely at minimum cost. Some of the characteristics of AH-25 are given in Table 1.

Moreover, as a hybrid UAV that could operate in both fixed-wing and Vertical Take-Off and Landing (VTOL) modes, the vehicle is expected to transit accurately and safely from one mode to the other. However, these requirements cannot be achieved without suitable flight dynamics model that would be used to design and analyze some critical systems such as the Flight Control System (FCS) of the aircraft. This paper provides a detailed description of the development of models that capture the dynamics of AH-25 UAV.

The paper is organized as follows. Section 1 is the introduction, Section 2 reviews the development of other UAV models, Section 3 presents the materials and methods that were used for the development of the AH-25 model, Section 4 includes presentation and discussion of obtained results, while Section 5 gives a conclusion on the work done.

2. RELATED WORK

Modelling is a prerequisite for most control systems design. A mathematical model that gives an accurate representation of the plant to be controlled is essential in the design of such systems. Therefore, it is imperative to develop a model that will capture

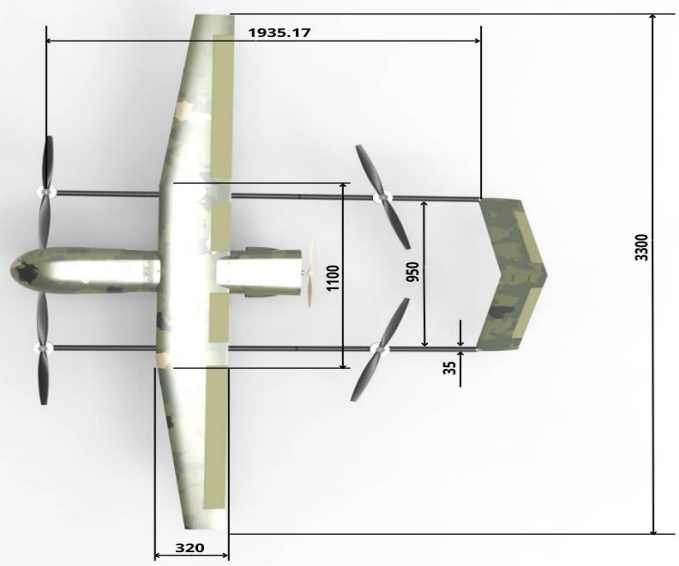

Figure 1. A rendered CATIA model of AH-25 Hybrid UAV with its dimension in millimeters

Table 1. Some characteristics of AH-25 UAV

Parameter	Value
Wing span	3.3 m
Endurance	>8 hours
Range	100 km
Max take-off mass	25 kg
Cruise speed	22 m/s
Maximum altitude	3000 m

the flight dynamics of UAVs over their entire flight envelop. Models could be developed through system identification which is suitable for black-box or grey-box systems or using first principle technique if there is complete knowledge on how the system operates [3-4]. The modelling of both conventional and hybrid UAVs has been discussed in relevant literature. Although a UAV is a complex system, the physics behind its operation is known. Therefore, its mathematical model could be obtained from both system identification and first principle derivation methods.

The most common method used for the modelling of conventional fixed-wing or rotary UAV is the Newton-Euler method [5]–[8]. In [5], the dynamical model that depicts the attributes of an over-actuated UAV was derived from first principle to analyze its behavior. Forces and moments that were produced by the motion of the propeller, as well as the inertial and gyroscopic effects that resulted from relative motion of the four propeller groups and the quadrotor body itself were all considered in the development of the model. Furthermore, a dynamic output linearization technique was designed, with the aid of the model, for trajectory control of the UAV. In a similar study [6], a mathematical model that captures the dynamics and kinematics of a quadcopter was developed using a hybrid coordinate system, which combined the earth-fixed and body-fixed reference frames. By employing the same approach, the external forces and moments acting on a fixed-wing UAV were modelled to represent the translational and rotational motions of the aircraft [7]. The developed nonlinear model was then linearized, using the small disturbance theory, to portray the steady state flight mode of the aircraft. In an effort to design a model-based adaptive control strategy for trajectory tracking of a quadrotor UAV [8], Newton equations were used to develop the dynamical model of the vehicle.

Developing a reliable flight dynamics model for hybrid UAV is challenging because its flight envelope is complex. The flight envelop for hybrid UAV is generally categorized into vertical mode, transition mode and straight level flight mode. Regarding rigid body dynamics of UAVs, two formulations are widely used depending on the UAV type. Few hybrid UAVs' modelling [9]–[11] used Euler-Lagrange method. Newton-Euler method was again found to be the prevalent approach for hybrid UAV rigid body modelling [12]–[17]. In [12], it was observed that proper modelling of all the modes in the complete flight envelope is crucial for the design of autonomous flight control system.

Depending on the type of hybrid UAV or mission, the orientation kinematics are expressed in either Euler angle formulation or Quaternion formulation [12]. Euler angle formulation are mostly used for convertiplanes while tail-sitters (operating in full flight envelope) kinematics are usually modelled using Quaternion formulation. The use of Quaternions for tail-sitter hybrid UAVs is mainly to avoid singularity effect when making transition from hover mode to level flight mode, or contrariwise.

The propulsion system model of hybrid UAVs is generally comprised of propeller aerodynamics and motor dynamics. Most works employed aerodynamic analyses to model propeller dynamics using simple models. For instance, [18] and [19] modelled aerodynamic forces and moments using quasi-steady equations. Most studies do not focus on motor dynamics for conventional UAVs. However, motor dynamics have significant effect in hybrid UAVs, especially during the transition phase. Transition phase is critical in hybrid UAVs for two reasons. One is that, the source of required lift changes; VTOL mode lift is from thrust generated by motors, while fixed-wing mode lift is mostly from aerodynamics of the wings. The other reason is change in the UAV's configuration resulting in change in direction of some forces. In [13], a 6-DOF model that depicts the dynamics of an unmanned aerial-underwater vehicle, based on the forces acting on the vehicle structure, was developed. The model was used to design an incremental dynamic inversion control scheme for attitude and altitude control of the vehicle.

Dual-system hybrid UAVs do not require specialized modelling for transition phase due to their configuration. Likewise, because tail-sitter has no special transition mechanism, extra modelling parameters are not required. Transition is usually achieved using control strategies. A unified model that captures the rotor, control surface and thrust vectoring dynamics of tail-sitter UAV was presented in [14].

For tilt-rotor and tilt-wing type UAVs, special models accounting for the tilting motion of the propulsion system are mostly adopted. In another study [17], a tilt-wing UAV was modelled to design a control system that regulates the hovering operation of the aircraft, and subsequently simulate its performance. The force and moments that depicts the hovering mode of the vehicle were derived from first principle with the aid of a rigid body diagram. The works in [20-22] all adopted a method in which the rotation of the left and right front propulsion system is represented with shaft tilting angles α-left and α-right. The tilting motion is defined by a rotation matrix (based on α-left and α-right values).

On the other hand, system identification is a modelling method that is used to represent the dynamics of aircraft [23-25]. The two modes: quadrotor and fixed-wing modes of a hybrid UAV were modelled as independent entities. An experimental method that involves measurement of the thrust generated by the vertical thrusters, when excited with different pulse-width-modulated (PWM) signal, was used for modelling the quadrotor dynamics. Although some parameters of fixed-wing mode were obtained experimentally, it was largely modelled using aircraft equations of motion. In an attempt to develop a flight simulator for a solar-powered UAV [24], a model that characterize the vehicle was developed. The model was developed with Datcom+Pro software, which was created for the design and analysis of aircraft. The geometric information of the vehicle was given to the software as an input file, and it produced the dimensionless stability derivatives of the aircraft. The model from Datcom+Pro was then loaded into MATLAB/Simulink platform with the aid of 'datcomimport' function. Additionally, system identification technique was used to model the longitudinal and lateral motions of a tail-sitter UAV [25]. Flight tests were then conducted to obtain the flight data that were used for the modelling. Flight simulation of the closed loop system, which involved a model predictive control strategy, showed that the identified models are robust enough for flight controller development. Moving mass mechanism is another modelling method that was identified in [26]. The forces and moments of multirotor UAV were modelled using the method. However, some model parameters such as moment of inertia were obtained through system identification.

3. MATERIAL AND METHOD

This section discusses the various methods and materials that were used in developing the models for AH-25 UAV. These include the simulation platform that was used for the development, and the modelling approaches that were utilized for both fixed-wing and VTOL modes of the UAV.

3.1 Simulation Platform

The MATLAB/Simulink software was used to develop the fixed-wing and VTOL models of the hybrid UAV. MATLAB was used because of the powerful tools it has for the design and analysis of engineering systems. Furthermore, the platform was used for simulating the open loop responses of the models to various inputs. Additionally, the results obtained were drawn using the plotting feature of the software.

3.2 Modelling

3.2.1 Fixed-Wing Model

The first step taken in the development of the fixed-wing model was the adaptation of the nonlinear 6DOF flat-earth equations of motion for a rigid body, which was based on Newton-Euler method. The equations are derived from Newton's second law of motion which models the external forces and moments acting on the aircraft and the Euler's kinematic representation, which depicts the attitude of the aircraft. The aircraft equations of motion that represents the 12 states of the vehicle are given as

$$\dot{X} = f(X,U) = \begin{bmatrix} \frac{1}{m}F^b - \omega_{b/e}{}^b X V^b \\ I_b{}^{-1}\left(M^b - \omega_{b/e}{}^b X I_b \omega_{b/e}{}^b\right) \\ H(\phi)\omega_{b/e}{}^b \\ T^e{}_{/b} V^b \end{bmatrix} \quad (1)$$

X is the state vector, F is the external forces vector, ω is the angular velocity vector, V is the linear velocity vector, I is the inertia matrix, M is the external moments vector, H is the angular momentum vector, and T is the symbol used for representation of transformation matrix. The subscripts/superscripts e and b represent the earth and body frames, respectively. The mathematical model was developed in the body frame. Also, the North-East-Down notation was used for the modelling. Equation (1) was adapted to suit the dynamics of AH-25 UAV by using the data gathered from the customer, experimental simulations used to obtain aerodynamic information and survey conducted on relevant literatures. Table 2 presents the data used for developing the model, and their respective sources.

The steps that were followed in developing a model specific to AH-25 UAV is described in the subsequent subsections.

Step 1: Control Limitation

The upper and lower limits of the control inputs were constrained to keep the aircraft within a controllable flight envelope. The values were obtained from conceptual design of the aircraft, and were included in the modelling to capture the entire dynamics involved. The limits are given in Table 3.

Table 2. Data used for fixed-wing model development

Data	Parameters	Sources
Nominal vehicle constants	Mass, structures information, mach number, cruise speed, control limits.	AH-25 specifications manual
Aerodynamic force coefficients	Coefficients of lift, drag and side force (C_L, C_D, C_Y).	XFLR5 software
Geometric information	Positions of center of gravity (CG) and engine	Weight and balance control technique
Moment of inertia and mean aerodynamic chord	Inertia and Mean Aerodynamic Chord (MAC)	Weight and balance control technique

Table 3. Limits imposed on control surfaces

Control surfaces	Lower limit	Upper limit
Ailerons	-20°	20°
Flaps	0°	30°
Ruddervators	-25°	25°
Throttle	0	1

Step 2: Intermediate Variables

The goal of this step is to ensure that all relevant variables used for the formulation of the model are functions of only the states and the control inputs as given by Equation (1). The 12 states that fully represents the aircraft's dynamics and kinematics are defined as follows:

$$\begin{bmatrix} x_1 \\ x_2 \\ x_3 \\ x_4 \\ x_5 \\ x_6 \\ x_7 \\ x_8 \\ x_9 \\ x_{10} \\ x_{11} \\ x_{12} \end{bmatrix} = \begin{bmatrix} \text{Forward Velocity}, u \\ \text{Side Velocity}, v \\ \text{Vertical Velocity}, w \\ \text{Roll Rate}, p \\ \text{Pitch Rate}, q \\ \text{Yaw Rate}, r \\ \text{Euler Roll Angle}, \phi \\ \text{Euler Pitch Angle}, \theta \\ \text{Euler Yaw Angle}, \psi \\ x-\text{direction} \\ y-\text{direction} \\ z-\text{direction} \end{bmatrix} \tag{2}$$

On the other hand, the control inputs that are used to achieve the desired operation are defined as follows.

$$\begin{bmatrix} U_1 \\ U_2 \\ U_3 \\ U_4 \\ U_5 \end{bmatrix} = \begin{bmatrix} \text{Rolling motion control input} \\ \text{Pitching motion control input} \\ \text{Yawing motion control input} \\ \text{Lift or drag increment contol input} \\ \text{Propulsion control input} \end{bmatrix} \tag{3}$$

All variables required for the development of the model are represented in form of the states and control inputs in Equations (2) and (3), respectively. Figure 2 shows how the states act on the vehicle using the North-East-Down frame. Furthermore, Table 4 shows how some of these variables are defined.

Step 3: Modelling the Dimensionless Aerodynamic Force Coefficients in the Stability Frame

Most of the aircraft's aerodynamic parameters were obtained from the XFLR5 software. The geometric information (in millimeters) of the aircraft was part of the input given to the software, and it subsequently output the aerodynamic parameters. The geometric representation of the vehicle is given by Figure 3. Furthermore, some of the parameters were culled from the empirical data of the aircraft category that the AH-25 belongs to. The formulae/values of the aerodynamic parameters, including the dimensionless force coefficients, are given in Table 5.

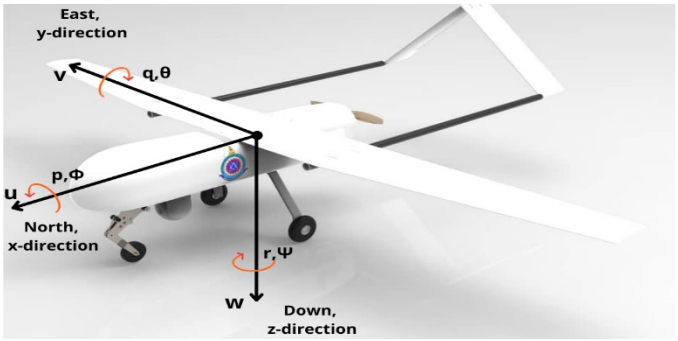

Figure 2. Description of the states acting on the vehicle using the North-East-Down frame

Table 4. Intermediate variables with their formulae

Variables	Formulae
Airspeed, V_A	$\sqrt{x_1^2 + x_2^2 + x_3^2}$
Angle of attack, α	$\tan^{-1}\left({}^{x_3}/_{x_1}\right)$
Angle of slip, β	$\sin^{-1}\left({}^{x_2}/_{\sqrt{x_1^2 + x_2^2 + x_3^2}}\right)$
Dynamic Pressure, Q	$0.6125(x_1^2 + x_2^2 + x_3^2)$
Angular velocity vector, $\omega = \begin{bmatrix} p \\ q \\ r \end{bmatrix}$	$\begin{bmatrix} x_4 \\ x_5 \\ x_6 \end{bmatrix}$
Translational velocity vector, $\begin{bmatrix} u \\ v \\ w \end{bmatrix}$	$\begin{bmatrix} x_1 \\ x_2 \\ x_3 \end{bmatrix}$

Table 5. Result of the aerodynamic analysis of the AH-25 UAV from XFLR5

Aerodynamic Parameters	Values/Formulae
Maximum coefficient of Lift (C_L)	$C_{L_{Max}} = 1.7$
Maximum C_L angle	11.2°
Zero lift angle	-3.6°
Angle of twist	-2°
Pitch moment coefficient at zero lift angle	$C_{M_O} = -0.057$
Drag polar for cruise condition	$C_D = 0.00973 + 0.0521C_L^2$
Drag polar for sea-level take-off	$C_D = 0.0109 + 0.0596C_L^2$
Drag polar for sea-level landing	$C_D = 0.0112 + 0.0569C_L^2$
Coefficient of side force	$C_Y = -0.83\beta + 0.1914U_3$

Step 4: Dimensionalization of Aerodynamic Forces in the Body Frame
The forces acting on the aircraft in the stability frame are given by

$$F^S = \begin{bmatrix} -F_D \\ F_Y \\ -F_L \end{bmatrix}^S = \begin{bmatrix} -C_D.Q.S \\ C_Y.Q.S \\ -C_L.Q.S \end{bmatrix}^S \tag{4}$$

S is the aircraft's planform area, *Q* represents dynamic pressure, while superscript/subscript *s* shows that the representation is in stability frame. F_D, F_Y and F_L are the drag force, side force and lift force respectively.

The forces are then rotated to the body frame using an appropriate rotation matrix, $T_{b/_s}(\alpha)$, as

$$F^b = T_{b/_s}(\alpha).F^S \tag{5}$$

where

$$T_{b/_s}(\alpha) = \begin{bmatrix} \cos\alpha & 0 & -\sin\alpha \\ 0 & 1 & 0 \\ \sin\alpha & 0 & \cos\alpha \end{bmatrix}$$

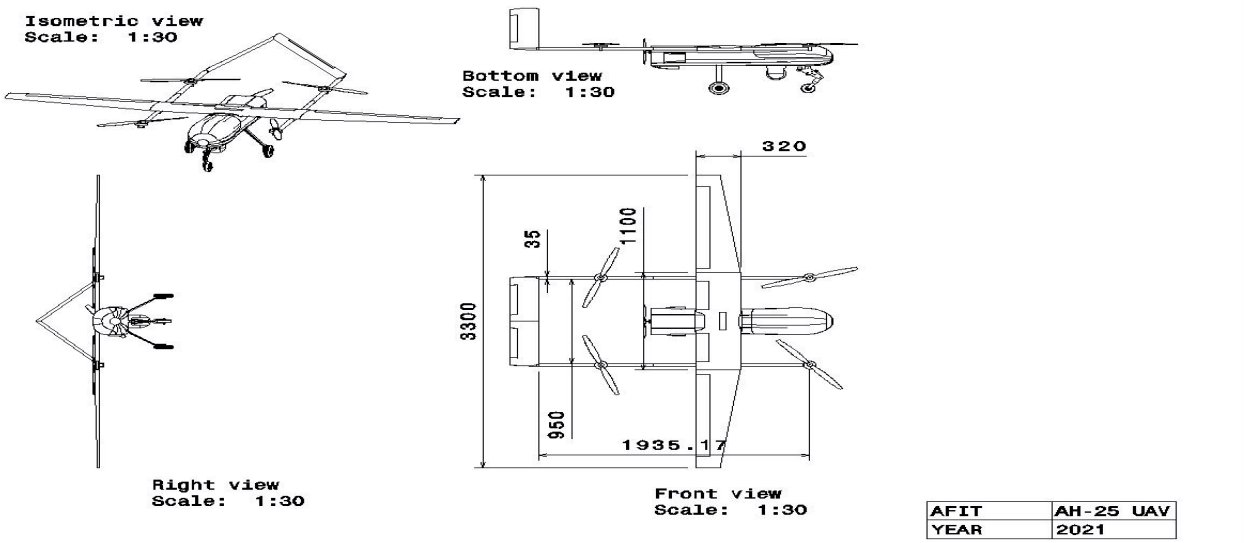

Figure 3. Geometric representation of AH-25 UAV

Step 5: Modelling Dimensionless Aerodynamic Moment Coefficients about Aerodynamic Center in the Body Frame
The equation of moment coefficient that was used in [27] is adopted for this design. The roll, pitch and yawing moment coefficients about the aerodynamic center in the body frame are formulated as

$$C^b_{MO_{ac}} = \begin{bmatrix} C_{L_{ac}} \\ C_{M_{ac}} \\ C_{N_{ac}} \end{bmatrix}^b = \eta + \frac{\partial C_m}{\partial X} + \omega^b_{b/_e} + \frac{\partial C_M}{\partial U} \begin{bmatrix} U_1 \\ U_2 \\ U_3 \end{bmatrix} \tag{6}$$

The terms in Equation (6) are defined as follows.

- η: Static moment effect.
- $\frac{\partial C_m}{\partial X}$: Dynamic angular rate behavior matrix, which indicates the effect of the angular rates on the moments.
- $\frac{\partial C_M}{\partial U}$: The matrix that captures the influence of the control inputs on the moments of the aircraft.
- $\omega^b_{b/_e}$:Rotational velocity vector in the body frame.
- $C^b_{MO_{ac}}$: Moment coefficient about the aerodynamic center in the body frame.
- $C^b_{L_{ac}}$, $C^b_{M_{ac}}$, $C^b_{N_{ac}}$: The roll, pitch and yawing moment coefficients, respectively.
- U_1, U_2, U_3: They are part of the control inputs defined in Equation (3).

Step 6: Dimensionalization of Aerodynamic Moments about Aerodynamic Center in the Body Frame
The aerodynamic moment about the aerodynamic center in the body frame is computed as

$$M^b_{A_{ac}} = C^b_{MO_{ac}}.Q.S.C \tag{7}$$

where *C* is the mean aerodynamic chord of the aircraft.

Step 7: Computation of Aerodynamic Moments about Center of Gravity in the Body Frame
The aerodynamic moment about the center of gravity was computed as

$$M^b_{A_{CG}} = M^b_{A_{ac}} + F^b_A.X.(r^b_{CG} - r^b_{ac}) \tag{8}$$

where r^b_{CG} is the position of the Center of Gravity (CG), while r^b_{ac} is the position of the aerodynamic center.

Step 8: Modelling the Propulsion effect
AH-25 is a single engine aircraft, which produces a forward force given by

$$F_1 = U_4.m.g \tag{9}$$

where *m* is the mass of the aircraft and *g* is the acceleration due to gravity. Therefore, the contribution of the force generated by the engine to the forces acting on the aircraft is depicted as

$$F_E^b = \begin{bmatrix} F_1 \\ 0 \\ 0 \end{bmatrix}^b \tag{10}$$

The moment generated by the engine about the center of gravity can be computed as

$$M_{E_{CG}}^b = \Delta t^b . X . F_E^b \tag{11}$$

where Δt^b is the distance between the CG and position of the engine.

Step 9: Modelling the Gravity Effect
The force of gravity acting on the aircraft in the earth frame is given by

$$F_g^e = m \begin{bmatrix} 0 \\ 0 \\ g \end{bmatrix}^e \tag{12}$$

The force was then transformed to the body frame using earth-to-body transformation matrix, $T_{b/e}$, as

$$F_g^b = T_{b/e} . F_g^e \tag{13}$$

The force of gravity does not cause any moment about the CG since it acts directly on it.

Step 9: Representation of Model in Explicit First-order Form
The fixed-wing dynamical model is then represented in explicit first order form using the computed moments and forces acting on the aircraft. The kinematical model was represented using Euler angle parameterization. The explicit first order form of the 12 states are given by

$$\begin{bmatrix} \dot{x}_1 \\ \dot{x}_2 \\ \dot{x}_3 \end{bmatrix} = \frac{1}{m} F^b - \omega_{b/e} . X . V^b \tag{14}$$

where

$$F^b = F_A^b + F_g^b + F_E^b \tag{15}$$

$$\begin{bmatrix} \dot{x}_4 \\ \dot{x}_5 \\ \dot{x}_6 \end{bmatrix} = I_b^{-1} \left(M_{CG}^b - \omega_{b/e}^b . X . I_b . \omega_{b/e}^b \right) \tag{16}$$

and

$$M_{CG}^b = M_{A_{CG}}^b + M_{E_{CG}}^b \tag{17}$$

$$\begin{bmatrix} \dot{x}_7 \\ \dot{x}_8 \\ \dot{x}_9 \end{bmatrix} = \begin{bmatrix} 1 & \sin\phi \tan\theta & \cos\phi \tan\theta \\ 0 & \cos\phi & -\sin\phi \\ 0 & \sin\phi / \cos\theta & \cos\phi / \cos\theta \end{bmatrix} \begin{bmatrix} x_4 \\ x_5 \\ x_6 \end{bmatrix}^b \tag{18}$$

$$\begin{bmatrix} \dot{x}_{10} \\ \dot{x}_{11} \\ \dot{x}_{12} \end{bmatrix} = T_{e/b} \begin{bmatrix} x_1 \\ x_2 \\ x_3 \end{bmatrix}^b \tag{19}$$

$T_{e/b}$ is the transformation matrix from body to earth frame. The 3D positions of the aircraft are represented in earth frame to have an accurate estimation of the vehicle from a reference location.

3.2.2 Trimming, Linearization and Decoupling of the Coupled Nonlinear Fixed-wing Model

The 12 nonlinear equations of motion that describe the kinematics and dynamics of AH-25 fixed-wing mode were given in Equations (14) - (19) in explicit first-order form. As a physical system, these are the equations that best represent the behavior of the aircraft. However, due to their complexity, they are difficult to use in designing controllers that would stabilize and improve the responses of an aircraft. Therefore, it is paramount to linearize and decouple the nonlinear equations to develop state-space and/or transfer function models, which are simpler and compatible for designing aircraft control loops. Thus, this section focuses on developing linear models that would be used for easier autopilot design. The linearized models give an approximate representation of the aircraft under specified conditions.

The 12 nonlinear coupled equations of motion can be linearized and decoupled into longitudinal motion, which includes pitch angle and forward velocity; and lateral motion, which includes side velocity, roll and yaw angles. Although element of coupling would still exist between the two decoupled motions, it could be appropriately handled by control algorithms meant to reject disturbances. The linear models are derived at trimming points, which is the name given to equilibrium points in flight dynamics.

The following steps were used for developing linear decoupled state-space model for the AH-25-UAV.

Step 1: Trimming

For any nonlinear system given by

$$\dot{x} = f(x, u) \tag{20}$$

where x is the system state vector, and u is the input vector. The system is said to be in equilibrium if:

$$f(x^*, u^*) = 0 \tag{21}$$

where x^* and u^* are the equilibrium or trim points. The linearized model would differ from one operating condition to another. Furthermore, the linearized model would only accurately represent the aircraft if it is operated within the vicinity of the operating point at which it was linearized. The trim conditions of a flight operation that is required to be linearized are based on the behavior of the states and inputs during the operation.

For steady state straight and level flight, the AH-25 has the following flight conditions:

$$X = [22\ 0\ 0\ 0\ 0\ 0\ 0\ 0\ 0\ 0\ 0\ -3000] \tag{22}$$

$$U = [0\ 0\ 0\ 0\ 0\ 0\ 0\ 0.8] \tag{23}$$

The state vector in Equation (22) and the control input vector in Equation (23) were obtained by substituting the appropriate aircraft's specification (as provided by Tables 1 and 3) into Equations (2) and (3). The MATLAB's *Trim* command was used for the trimming, and it solves Equation (21) with the conditions given to provide the trimming points for the straight and level flight, which are represented by Equations (24) and (25).

$$X^* = [159\ 0\ 4\ 0\ 0\ 0\ 0\ -0.2\ 0\ 0\ 0\ -3000] \tag{24}$$

$$U^* = [0\ 0\ 0\ 0\ -0.0622\ -0.0622\ 0.1095] \tag{25}$$

Step 2: Decoupling and Linearization

To obtain the lateral model of the aircraft, the longitudinal states *u, w, θ, q, x, z* are equated to zero. The lateral control inputs are U_1 and U_3. On the other hand, the lateral states *v, ϕ, ψ, p, r, z* are equated to zero to obtain the longitudinal motion model of the aircraft. For longitudinal motion model, the control inputs are U_2, U_4 and U_5.

The general state-space model is given by

$$\dot{x} = Ax + Bu \tag{26}$$

where A is the system matrix and B is the control matrix. The trim points can be obtained by equating Equation (20) to zero, and solving for x^* and u^*. The trim points can then be used to linearize the system with the aid of Taylor series expansion method. The approximate linear model after applying the expansion method is

$$\tilde{\dot{x}} = \frac{\partial f(x^*, u^*)}{\partial x}\tilde{x} + \frac{\partial f(x^*, u^*)}{\partial u}\tilde{u} \tag{27}$$

where $\frac{\partial f(x^*,u^*)}{\partial x}$ and $\frac{\partial f(x^*,u^*)}{\partial u}$ are Jacobian matrices. Comparing Equation (26) with Equation (27), $A = \frac{\partial f(x^*,u^*)}{\partial x}$ and $B = \frac{\partial f(x^*,u^*)}{\partial u}$. However, the linear models were easily obtained without going through the tedious task of solving the Jacobian matrices by using the *linmod* MATLAB command. The lateral state space matrices are given by

$$\tilde{\dot{x}} = \frac{\partial f(x^*, u^*)}{\partial x}\tilde{x} + \frac{\partial f(x^*, u^*)}{\partial u}\tilde{u} \tag{27}$$

$$A_{Lat} = \begin{bmatrix} -0.3034 & -6.9799 & -15.0389 & 8.8983 & 0 & 0 \\ -4.9739 & -8.0954 & 4.2172 & 0.0000 & 0 & 0 \\ 6.9571 & 1.1343 & -4.1955 & 0 & 0 & 0 \\ 0 & 1 & -0.4641 & 0 & 0 & 0 \\ 0 & 0 & 1.1025 & 0 & 0 & 0 \\ 1 & 0 & 0 & 6.9799 & 16.5797 & 0 \end{bmatrix} \tag{28}$$

$$B_{Lat} = \begin{bmatrix} 0 & 0 & -0.5801 & 0.5801 \\ 14.2040 & -14.2040 & -7.1008 & 7.1008 \\ -0.9772 & 0.9772 & 0 & -13.3178 \\ 0 & 0 & 0 & 0 \\ 0 & 0 & 0 & 0 \\ 0 & 0 & 0 & 0 \end{bmatrix} \tag{29}$$

The longitudinal model's state and control matrices were computed as

$$A_{Lon} = \begin{bmatrix} -0.3544 & 0.7562 & 6.9799 & -8.8983 & 0 & 0 \\ -1.1083 & 0.1617 & 15.0389 & 4.1299 & 0 & 0 \\ -11.5319 & -24.8466 & -56.4871 & 0 & 0 & 0 \\ 0 & 0 & 1 & 0 & 0 & 0 \\ 0.9071 & -0.4210 & 0 & 0 & 0 & 0 \\ 0.4201 & 0.9071 & 0 & -16.5797 & 0 & 0 \end{bmatrix} \tag{30}$$

$$B_{Lon} = \begin{bmatrix} 0 & 0 & 0 & 9.81 \\ 0 & 0 & 0 & 0 \\ -247.5652 & -247.5652 & -247.5652 & -247.5652 \\ 0 & 0 & 0 & 0 \\ 0 & 0 & 0 & 0 \\ 0 & 0 & 0 & 0 \end{bmatrix} \tag{31}$$

3.2.3 VTOL Mode Modelling

For the VTOL mode modelling, the multicopter model developed by Beihang Flight Control Group [28] was adapted. The model is an amalgam of several sub-models. It contains the following models:

- Motor model that describes the dynamics of the motor used
- Force and moments model that captures the external forces and moments acting on the vehicle
- Kinematics model which portrays the motion of the aircraft
- Environmental model that represents the condition of the environment
- Fault model that is used to test the behavior of the vehicle upon injection of disturbances/uncertainties
- Battery model that depicts the discharge rate of the propulsion unit
- Output interface model which stores the response of the vehicle in the specified form.

The block diagram of the different parts of the model is shown in Figure 4.

The model is reconfigurable such that by changing the model parameters, multicopter of varying sizes and configurations could be modelled [28]. This unique feature was utilized for the development of the VTOL model for the AH-25 UAV. The parameters that were changed to suit the dynamics of the AH-25 VTOL UAV mode were mostly the parameters of the selected motor and propeller. The T-motors' P80 KV170 motor and G30*15 Carbon fiber propeller were used for the design of the VTOL mode. Some of the parameters needed for the modelling, which are presented in Tables 6 and 7, are specified by the manufacturer of the motor and propeller utilized. The required parameters for development of the mathematical model that are not specified were computed as presented in the upcoming subsections.

Table 6. P80 KV170 motor specifications

Parameters	Values
Internal sesistance	17-23 ohms
Weight/Motor	0.65 kg
Maximum angular speed	3255 rpm
Shaft diameter	15 mm

Table 7. Propeller parameters

Parameters	Values
Maximum thrust	323.73 N
Rotational speed	1300 – 3000 rpm
Operating temperature	-45°C – 65°C
Propeller type	2 blades
Weight (Single Blade)	0.097 kg
Diameter	762 mm

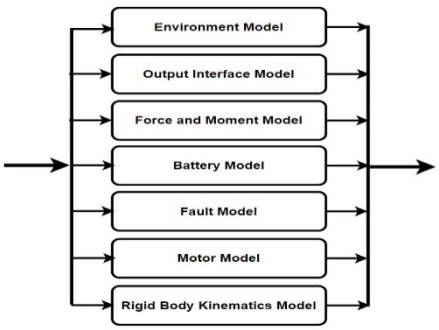

Figure 4. Block diagram of the VTOL model

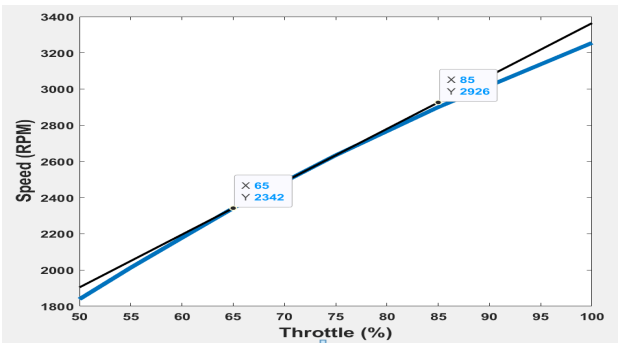

Figure 5. Motor speed-throttle curve

VTOL Model Parameters Computation

The needed motor parameters that were not given, and are necessary for the model development are computed in this subsection.

1) Motor Speed-Throttle Slope (M_{STS})

This parameter was computed using the speed-throttle curve that was plotted from the data given by the manufacturer. The plot that shows the curve, together with a line that is tangent to the curve, is given by Figure 5. It is found that

$$M_{STS} = \frac{\Delta Speed}{\Delta Throttle} = \frac{2926 - 2342}{0.85 - 0.65} = 2920 \ {}^{\text{rev}}/_{\text{min}}$$

$$M_{STS} = 2920 * \frac{2\pi}{60} \ {}^{\text{rad}}/_{\text{s}} = 305.8 \ {}^{\text{rad}}/_{\text{s}}$$

2) Moment of Inertia of Motor Rotor + Propeller (I_{mp})

$$I_{mp} = \frac{M_{mp}.r^2}{2} \tag{32}$$

$$\text{M}_{\text{mp}} = \text{Mass of motor} + \text{Mass of Propeller}$$

$$\text{M}_{\text{mp}} = 0.65 + (0.097 * 2) = 0.844 \text{ kg}$$

$$\text{r} = \left(\frac{15}{2}\right) * 10^{-3} = 0.0075 \text{ m}$$

$$\text{I}_{\text{mp}} = \frac{0.844 * 0.0075^2}{2} = 0.000024 \text{ kgm}^2$$

3) Propeller Moment Coefficient, C_{pm}

$$C_{pm} = \frac{Torque}{(Angular\ Velocity)^2} \tag{33}$$

$$Torque = \text{Thrust} * \text{Propeller Radius} = 323.73 * (381 * 10^{-3}) = 123.34 \text{ Nm}$$

Therefore,

$$C_{pm} = \frac{123.34}{(314.16)^2} = 0.00125 \text{ Nm}/(\frac{\text{rad}}{\text{s}})^2 \tag{34}$$

4) Propeller Thrust Coefficient, C_{tm}

$$C_{tm} = \frac{Thrust}{(Angular\ Velocity)^2} \tag{34}$$

$$C_{tm} = \frac{323.73}{(314.16)^2} = 0.0033 \text{ N}/(\frac{\text{rad}}{\text{s}})^2$$

3.3 Modelling

The mean values of the fixed-wing model's steady state error, settling time and rise time are the open-loop time response metrics that were evaluated to observe the performance of the model. The metrics are defined as follows:

- Steady state error: This is the discrepancy between the output of the model and the desired output at steady state.
- Rise time: the time taken by the output of the model to rise from 10% to 90% of the final value.
- Settling time: the time taken by the output of the system to reach and stay between 98% to 102% of the final value

4. RESULT AND DISCUSSION

In this section, the results obtained from the designed models were presented and subsequently discussed.

4.1 Nonlinear Coupled 6-DOF Fixed-Wing Model

The model from preceding sections was coded and simulated in the MATLAB/Simulink environment to observe its stability. The nonlinear coupled 6-DOF fixed-wing model's MATLAB block diagram is given by Figure 6. It is the block diagram that implemented Equations (14)-(19), with the limits in Table 3 imposed on the control inputs. To observe the operation of the

model, it was commanded to pitch up, while moving forward, by deflecting the ruddervator symmetrically as could be seen from the inputs used in Figure 7. It could be seen that all states, such as roll and yaw angles/rates, that should not be changing while the model is climbing remains at zero. Conversely, it could be observed from Figure 7 that states related to the forward movement and ascent of the model, such as forward velocity, *x*-direction, pitch angle/rate and *z*-direction, corresponds well to the input given. Since North-East-Down notation was used, the altitude of the model is the negative of the *z*-direction. Therefore, the model is actually ascending and not descending as may be inferred from the figure. Although there are some oscillations in the transient response of the model's states, they are bounded and could be reduced and/or neglected by a control system. Hence, the model matches the actual operation of an aircraft.

The mean performance metrics of the model's response to various inputs were computed. The model was found to have a steady state error of 1.33%, a rise time of 2 s and a settling time of 40 s. The stability of the model was examined by perturbing it at some instances of its operation to observe whether it would recover from the perturbations. As could be seen from Figure 8, the model is initially cruising before it was rolled by deflecting the ailerons asymmetrically at 30 s. The deflection was then removed at 35 s to observe the corresponding response of model. At 30 s states that are related to the rolling motion of the model such as the side velocity, roll rate/angle, yaw rate/angle and *y*-component, were found to be affected by the deflection. However, at 35 s when the deflection was removed, most of the states tend to return to their original states. Only the *y*-component and yaw rate did not return to their initial states. However, that is understandable because the heading of the aircraft is changed by the rolling motion it went through. Therefore, it can be concluded that the aircraft is stable.

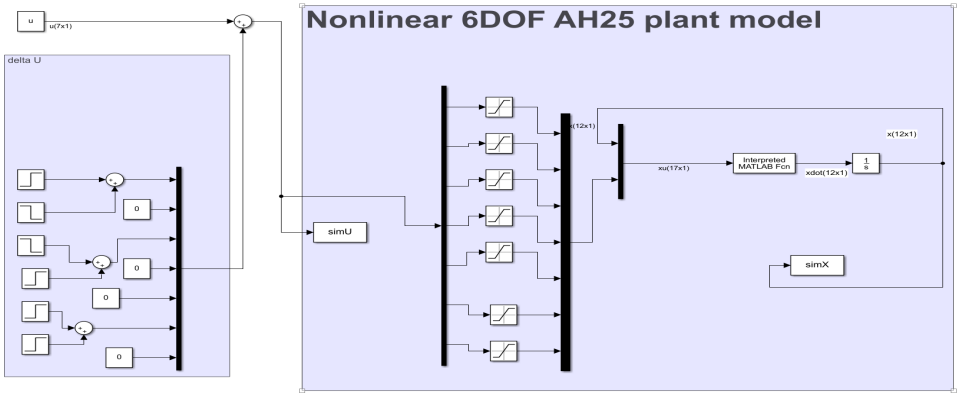

Figure 6. MATLAB block diagram of the nonlinear 6-DOF fixed-wing model

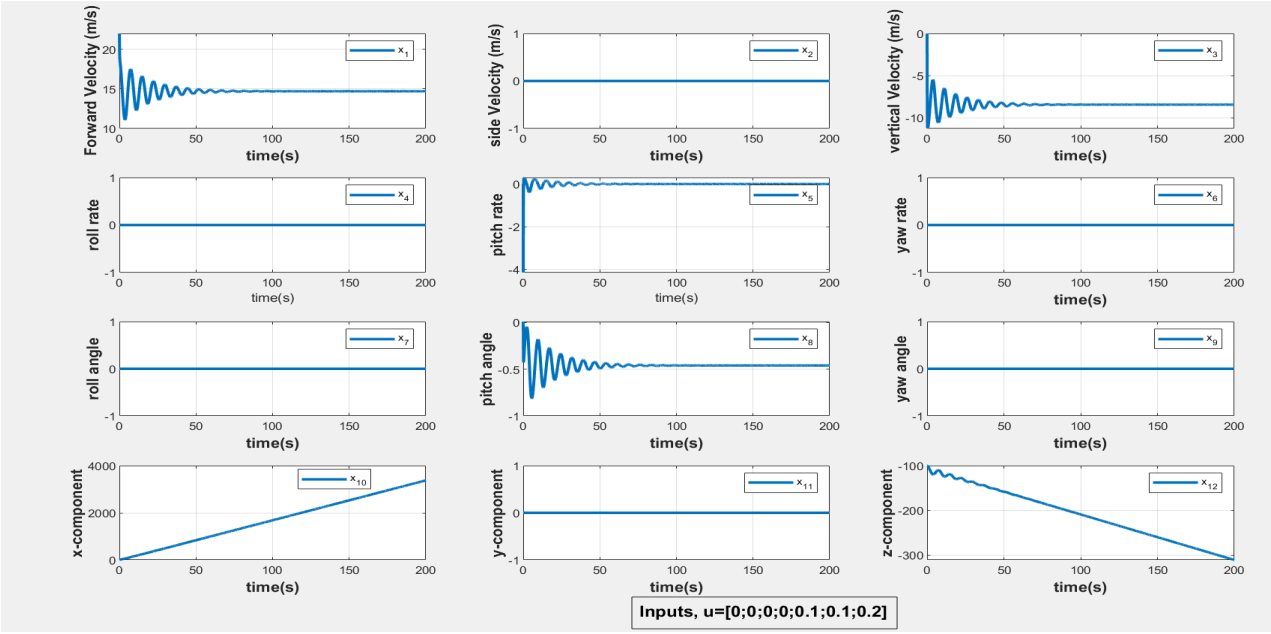

Figure 7. Observing the operation of the nonlinear 6-DOF fixed-wing model

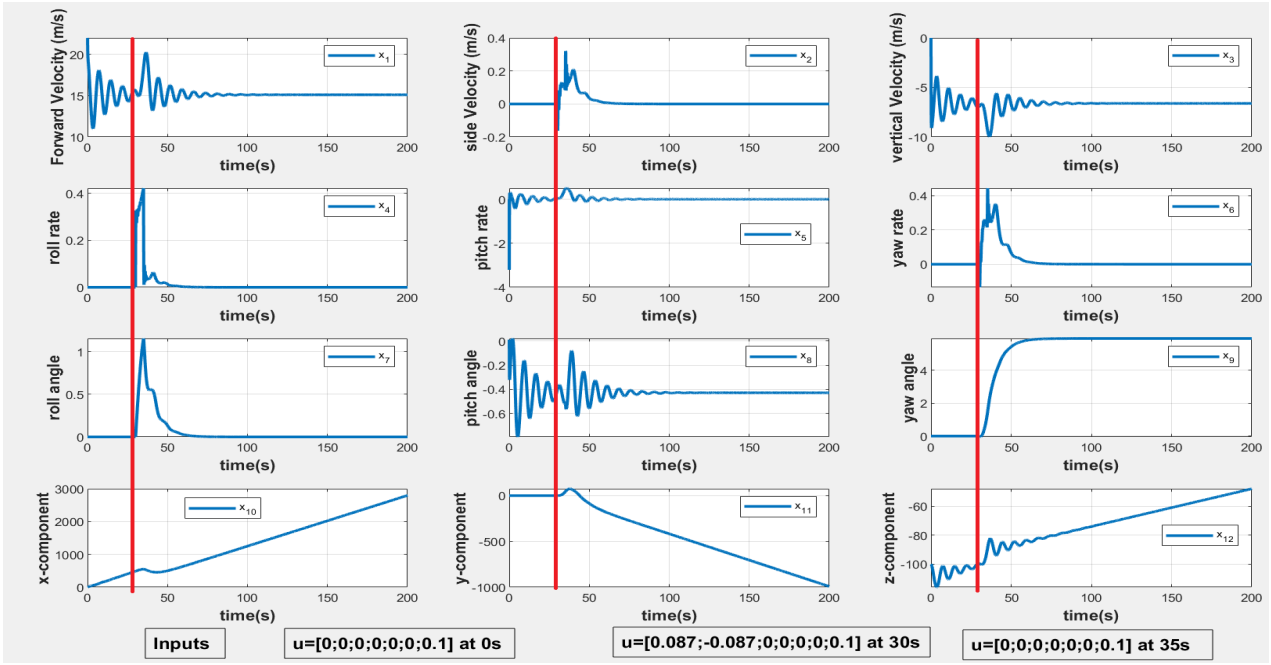

Figure 8. Testing the stability of the nonlinear 6-DOF fixed-wing model

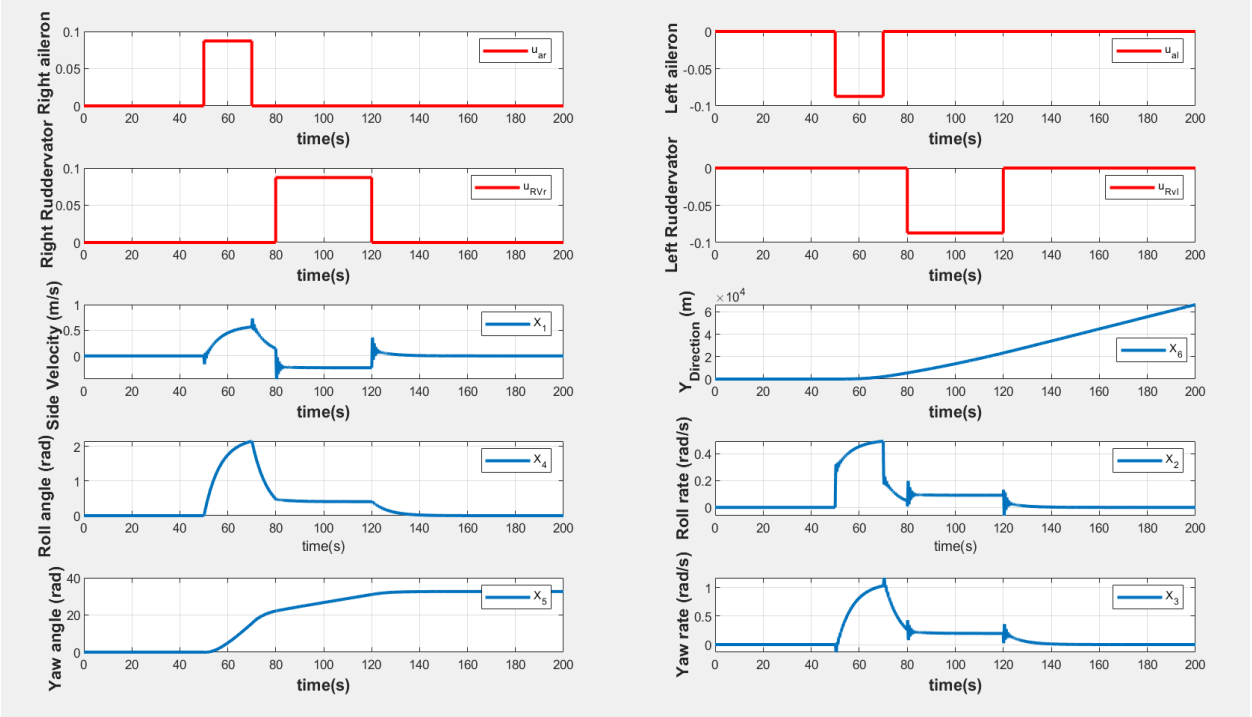

Figure 9. Testing the stability of the lateral motion model

4.2 Linear Decoupled Models

The stability of both lateral and longitudinal motion models was tested by simulating the models with appropriate control inputs. In Figure 9, the stability of the lateral model was tested by deflecting the ailerons and ruddervators, asymmetrically, at different instances. The ailerons were deflected at 50 s, and the deflections were removed at 70 s. On the other hand, the ruddervators were deflected at 80 s, and the deflections were removed at 120 s. In all cases, the lateral states of the model correspond to actual stable operation of an aircraft by recovering from the perturbations.

In Figure 10, the model was initially cruising and pitching up. The ruddervators were then symmetrically deflected at 80 s to increase the rate at which the pitching occurs. The deflections were removed at 120 s. The results obtained conform with the objective. It could be seen that at 80 seconds, the vertical velocity, pitch angle/rate and climbing of the aircraft increased. However, at 120 s the states returned back to their initial states. These results showed that the longitudinal and lateral models of the aircraft depict its motion.

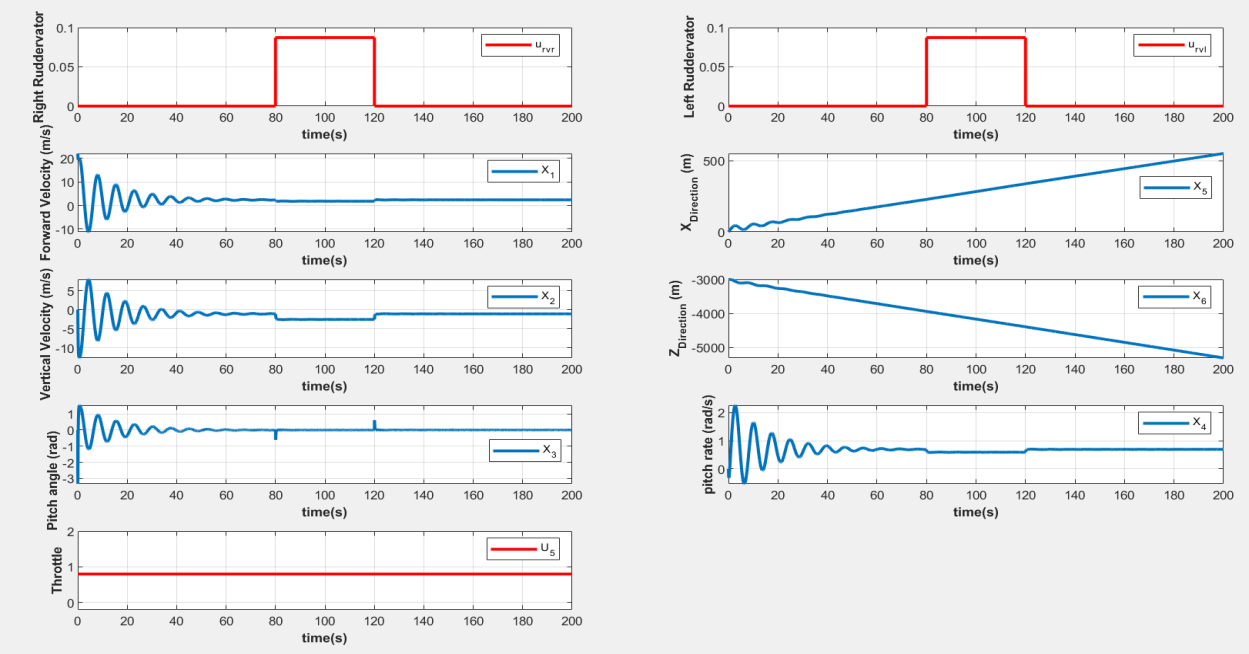

Figure 10**:** Testing the stability of the longitudinal motion model.

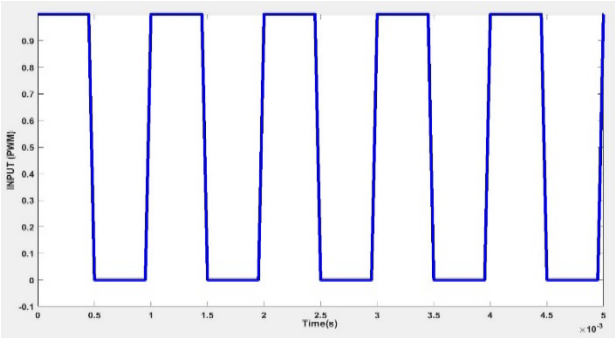

Figure 11: Input given to the VTOL model

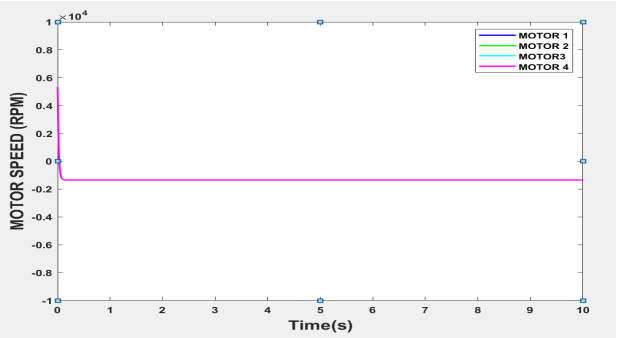

Figure 12. Angular speed of the four motors. The speed is the same, that is why all other colors are superimposed and only the last color appears

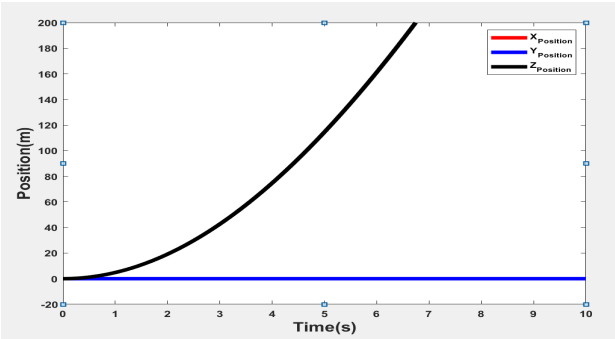

Figure 13. 3D directions of the aircraft over time

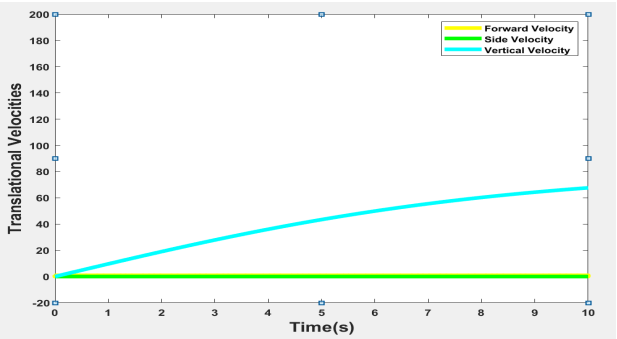

Figure 14. Translational velocities of the aircraft over time

4.3 VTOL Model

The open-loop response of the VTOL model was observed after exciting it with a pulse width modulated (PWM) signal that is given in Figure 11. The angular speed of the four motors in the VTOL system was found to be 1000 RPM in the clockwise direction as shown in Figure 12. It was the motor speed that produced the thrust, which translated into the translational positions and velocities of the UAV during vertical take-off as shown in Figures 13 and 14, respectively. The model conformed to performance specification of a VTOL system. As could be seen from Figures 13 and 14, only the altitude and vertical velocity changed over time, which corresponds to the operation of the motors.

5. CONCLUSION

This paper provides modelling of AH-25 UAV in the fixed-wing and VTOL modes. The models were implemented and tested for conformance to aircraft operation and stability in the MATLAB design environment. The fixed-wing model was decoupled, trimmed and linearized for easier design of aircraft systems such as FCS. The results obtained showed that the models are stable for the intended purposes and operate according to AH-25 UAV specifications. Since the modes of the aircraft were modelled in this work, there is need to design a transition algorithm that would safely switch from one mode to another during the operation of the hybrid vehicle. Therefore, future work could focus on the development of transition algorithms for the two modes

ACKNOWLEDGMENT

This research was sponsored by Tertiary Education Trust Fund (TETFUND, Nigeria) Institutional-Based Research (IBR 2019).

REFERENCES

[1] G. Lee and C. O. Kim, Autonomous control of combat unmanned aerial vehicles to evade surface-to-air missiles using deep reinforcement learning, *IEEE Access*, 8, 2020, 226724-226736.

[2] C. Kerr, R. M. Jaradat and N. U. I. Hossain, Battlefield mapping by an unmanned aerial vehicle swarm: applied systems engineering processes and architectural considerations from system of systems, *IEEE Access*, 8, 2020, 20892-20903.

[3] R. Gill and R. D. Andrea, Computationally efficient force and moment models for propellers in UAV forward flight applications, *Drones*, 3(4), 2019, 77.

[4] J. Hermann, R. Distasio and A. Tkatchenko, First-principles models for van der waals interactions in molecules and materials: Concepts, theory, and applications, *Chemical Reviews*, 117(6), 2017, 4714-4758.

[5] M. Ryll, H. Bülthoff and P. Giordano, A novel overactuated quadrotor unmanned aerial vehicle: modeling, control, and experimental validation, *IEEE Transactions on Control Systems Technology,* 23, 2015, 540-556.

[6] Z. Benić, P. Piljek and D. Kotarski, Mathematical modelling of unmanned aerial vehicles with four rotors, *Interdisciplinary Description of Complex Systems*, 14, 2016, 88-100.

[7] E. A. Ahmad, A. Hafez, A. N. Ouda, H. E. H. Ahmad and H. M. Abd-Elkadir, Modelling of a small unmanned aerial vehicle, *Advances in Robotics and Automation*, 4(1), 2015, 1000126.

[8] S. Islam, P. Liu and A. El Saddik, Robust control of four-rotor unmanned aerial vehicle with disturbance uncertainty, *IEEE Transactions on Industrial Electronics*, 62, 2015, 1563-1571.

[9] J. Escareno, S. Salazar-Cruz and R. Lozano, Attitude stabilization of a convertible mini birotor, *IEEE Conference on Computer Aided Control System Design, IEEE International Conference on Control Applications, IEEE International Symposium on Intelligent Control*, Munich, Germany, 2006, 2202-2206.

[10] J. Escareno, S. Salazar and R. Lozano, Modelling and control of a convertible VTOL aircraft, *Proceedings of the 45th IEEE Conference on Decision and Control*, San Diego, USA, 2006, 69-74.

[11] A. Sanchez, J. Escareño, O. Garcia and R. Lozano, Autonomous hovering of a noncyclic tiltrotor UAV: modeling, control and implementation, *IFAC Proceeding Volumes*, 41(2), 2008, 803-808.

[12] S. Saeed, A. B. Younes, C. Cai and G. Cai, A survey of hybrid unmanned aerial vehicles, *Progress in Aerospace Sciences*, 98, 2018, 91-105.

[13] G. Chen, A. Liu, J. Hu, J. Feng and Z. Ma, Attitude and altitude control of unmanned aerial-underwater vehicle based on incremental nonlinear dynamic inversion, *IEEE Access*, 8, 2020, 156129-156138.

[14] Y. Ke, K. Wang and B. Chen, Design and implementation of a hybrid UAV with model-based flight capabilities, *IEEE/ASME Transactions on Mechatronics*, 23(3), 2018, 1114-1125.

[15] M. Allenspach and G. J. J. Ducard, Nonlinear model predictive control and guidance for a propeller-tilting hybrid unmanned air vehicle, *Automatica*, 132, 2021, 109790.

[16] M. Mehndiratta, E. Kayacan, M. Reyhanoglu and E. Kayacan, Robust tracking control of aerial robots via a simple learning strategy-based feedback linearization, *IEEE Access*, 8, 2020, 1653-1669.

[17] E. Small, E. Fresk, G. Andrikopoulos and G. Nikolakopoulos, *Modelling and control of a tilt-wing unmanned aerial vehicle*, *24th Mediterranean Conference on Control and Automation*, Athens, Greece, 2016.

[18] S. Kohno and K. Uchiyama, Design of robust controller of fixed-wing UAV for transition flight, *International Conference on Unmanned Aircraft Systems (ICUAS)*, Orlando, USA, 2014, 1111-1116.

[19] J. T. Vandermey, *A tilt rotor UAV for long endurance operations in remote environments*, Master Thesis, Massachusetts Institute of Technology, USA, 2011.

[20] C. Papachristos, K. Alexis and A. Tzes, Design and experimental attitude control of an unmanned tilt-rotor aerial vehicle, *15th International Conference on Advanced Robotics (ICAR)*, Tallinn, Estonia, 2011, 465-470.

[21] X. Fang, Q. Lin, Y. Wang and L. Zheng, Control strategy design for the transitional mode of tiltrotor UAV, *IEEE International Conference on Industrial Informatics*, Beijing, China, 2012.

[22] S. Park, J. Bae, Y. Kim and S. Kim, Fault tolerant flight control system for the tilt-rotor UAV, *Journal of Franklin Institute*, 350(9), 2013, 2535-2559.

[23] J. Kalpa Gunarathna and R. Munasinghe, Development of a quad-rotor fixed-wing hybrid unmanned aerial vehicle,

Moratuwa Engineering Research Conference, 2018, 72-77.

[24] M. Enomoto and Y. Yamamoto, Modelling, simulation and navigation experiments of unmanned aerial vehicle, *IEEE International Conference on Mechatronics and Automation*, Beijing, China, 2015.

[25] W. Zhou, S. Chen, C. W. Chang, C. Y. Wen, C. K. Chen and B. Li, System identification and control for a tail-sitter unmanned aerial vehicle in the cruise flight, *IEEE Access*, 8, 2020, 218348-218359.

[26] T. Haus, M. Orsag and S. Bogdan, Mathematical modelling and control of an unmanned aerial vehicle with moving mass control concept, *Journal of Intelligent & Robotic Systems*, 88, 2017, 219-246.

[27] M. Huzmezan and J. Maciejowski, Original: english GARTEUR/TP-088-20 April 4, 1997, 1997.

[28] Q. Quan, X. Dai and S. Wang, *Multicopter Design and Control Practice: A Series Experiments Based on MATLAB and Pixhawk*, Springer, 2020.